September 25th - 28th, 2017
INTERFACES
architecture . engineering . science IASS 2017 hamburg

Proceedings of the IASS Annual Symposium 2017
"Interfaces: architecture.engineering.science"
25 - 28th September, 2017, Hamburg, Germany
Annette Bögle, Manfred Grohmann (eds.)

Ceramic 3D printing – The future of brick architecture

Paulo J.S. CRUZ*, Ulrich KNAACK[a,b], Bruno FIGUEIREDO[c], Dennis de WITTE[b]

* Lab2PT, School of Architecture, University of Minho
4800-058 Guimarães, Portugal
pcruz@arquitetura.uminho.pt

[a] Design of Construction, Faculty of Architecture and the Built Environment, Delft University of Technology
[b] Institute of Structural Mechanics and Design, Faculty of Civil and Environmental Engineering, Technische Universität Darmstadt
[c] Lab2PT, School of Architecture, University of Minho

Abstract

The advent of Additive Manufacturing (AM) of ceramic, brought unprecedented possibilities for the building industry while exploring and incorporating components with specific design requirements. It definitively reshaped and expanded the boundaries of what's possible to achieve with masonry construction and opened new domains, with multiple angles of study and experimentation and with a large industrial potential.

This paper presents the main challenges and outcomes of an ongoing research project aiming to explore the integration of digital additive manufacturing techniques in the architectural design and production processes of free-form stoneware bricks for building envelopes. The project uses a clay extruding printer, Lutum®, built by the company Vormvrij available at the Advanced Ceramics R&D Lab, at the Design Institute of Guimarães and at Technische Universität Darmstadt. The path, material flow and printing speed of the printing process are defined digitally. The movement speed, extrusion flow and the air pressure can be controlled manually to adapt the specific printing process to the characteristics of the clay during the printing process itself. The widely accepted Pfefferkorn method has been extensively used to evaluate and control the plasticity of the stoneware used.

Keywords: Additive manufacturing, ceramic 3D printing, robocasting, clay extrusion, brick architecture, building envelopes, parametrical drawing, accuracy, print resolution, material mixtures.

1. Introduction

The past decades have been by a rediscovery of architectural ceramics - a material system that has long served merely as a practical surface treatment for buildings, but that is now coming into its own as a multi-functional, intensely aesthetic boundary layer for buildings (Bechthold *et al.* [1]).

The possibility to additively produce ceramic components brings new opportunities for the building industry to explore the possibilities of incorporating components with specific design requirements (Knaack *et al.* [2]). This means that, the research path to define these innovative systems and production methodologies is still in an embryonic stage, but it will reshape and expand the boundaries of what is achievable with masonry construction. It will define new domains, with multiple disciplines with a vast industrial potential to be studied and experimented.

There are still challenges to overcome before mass customisation of ceramic components becomes an innovative technology in the building industry to: use of computational design tools regarding methodologies for the production of optimised customised ceramic building components by use of AM;

redefine construction and assembly systems in order to potentiate the use of ceramic customised solutions; enhance ceramics features, by considering multi-functional applications.

AM allows direct and accurate construction of customised and multifunctional applicable building components with significant applications in architecture (Knaack *et al.* [3]). Recent experiments showed the application of ceramic materials as a contemporary solution for architectural production, enabling new uses and challenging functions, namely by discretising free-form geometries in components (Peters [4], [7]), integrating flexible interlocking connections (Sabin *et al.* [5]) and adding new performative and infra-structural features [6, 8].

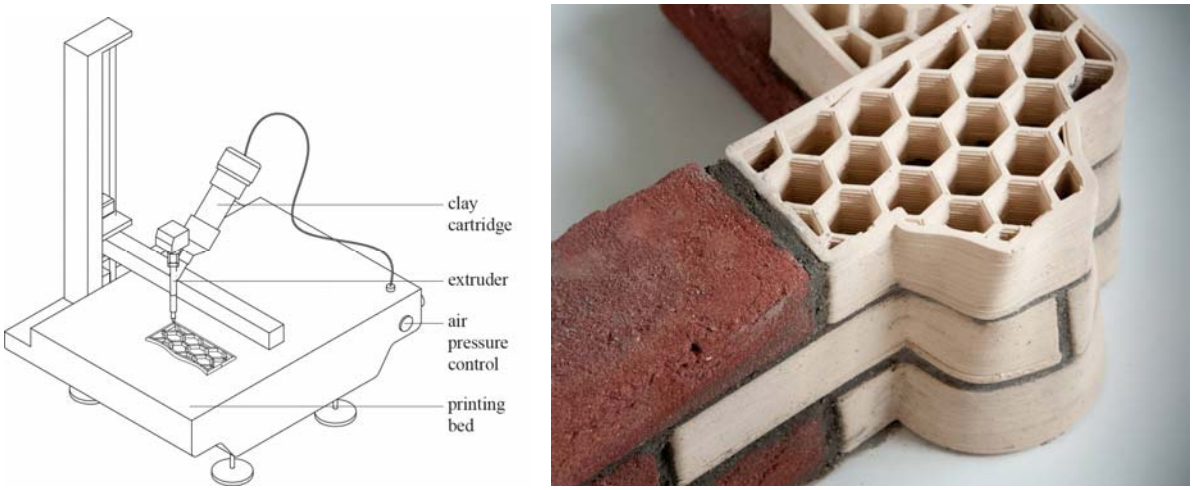

Figure 1: Lutum® 3D clay printer schema and a free-form ceramic corner bricks

This paper focuses on three main topics that describe the methodology of the ongoing research: the relation of the plasticity of the ceramic material on the performance of AM processes; to calibrate printing parameters in order to minimise deviations between 3D digital models and additive manufactured models; to define computational models that can be used for the generation of customised designs of stoneware bricks for the built environment, which focusses on the constraints regarding form and the physical restrictions of additive manufacturing of ceramic itself.

The Lutum® 3D clay printer used (Figure 1), can be referred to as a CNC machine with three movement axies that has a paste extruder fed by a pressurised clay cartridge mounted on it.

2. Deriving the stoneware's plasticity for additive manufacturing

In the processing of clay-based materials, plasticity is an essential property which determines how a ceramic mass is converted into a desired shape by the application of pressure (Andrade *et al.* [9]).

Several measuring techniques and devices are available to determine the optimal water content in a clay body required to allow this body to be plastically deformed by shaping. The widely accepted Pfefferkorn method has been extensively used in this research to evaluate and control the plasticity of the stoneware used. It determines the amount of water required to achieve a 30% reduction in height in relation to the initial height of the test body under the action of a standard mass (Pfefferkorn [10]).

Measuring plasticity according to Pfefferkorn is based on the principle of impact deformation. A defined sample with a diameter of 33 mm and an initial height of 40 mm, produced either manually or by extrusion, is deformed by a free-falling plate with a mass of 1.192 kg. The initial height is related to the impact deformation height, the result of which is the ratio of deformation. As a rule, this measurement is taken with bodies with varying moisture content.

Figure 2: Pfefferkorn test apparatus

The results are expressed as graphs showing height reduction as a function of moisture content. The ratios of deformation or the impact deformation heights (H_0, initial height; H_f, final height) are plotted against the moisture content. The steeper the curve, the "shorter" the body, i.e. the more the body its plasticity reacts to variations of the moisture content.

The Pfefferkorn method was adopted to compare the plasticity of three different ceramic materials: Gres-130-MP, a ceramic paste normally applied in manual and mechanical processes, whose plasticity can vary from order to order [11]; Gres-Art13-AT, a powdered stoneware for processing into ceramic paste normally used for bonding ceramic pieces [12]; Creaton No. 208, a powdered stoneware for processing into ceramic paste normally used for manual and mechanical works [13].

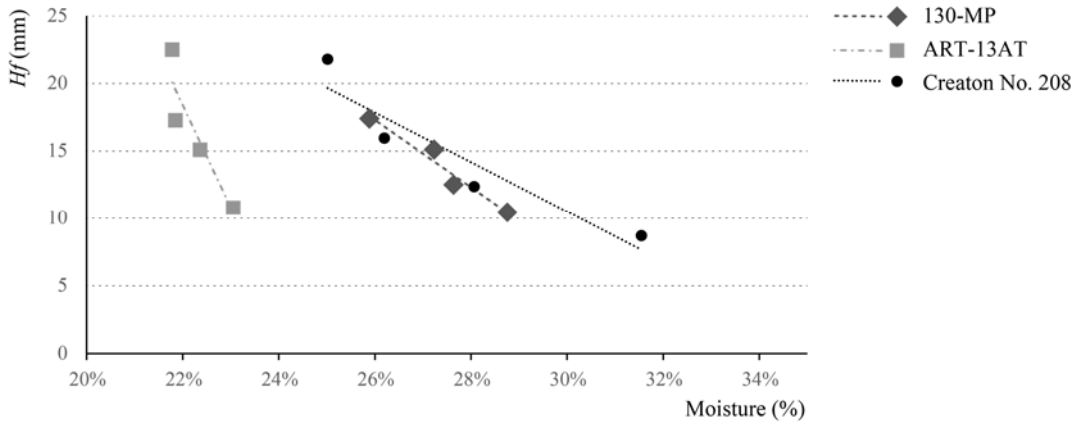

Figure 3: Pfefferkorn chart results

To carry out the tests with the powdered stoneware samples, there was initially water added to the stoneware to obtain a water content of 20wt% in the mixture. The water content was slightly increased during the tests and three cylindrical specimens were made after water addition. The final height of each individual specimen was measured directly after each Pfefferkorn test. The weight of the specimens was also recorded before and after desiccating in an electric oven, to be able to calculate the moisture content of each specimen. The tests were carried out until the mean height of the samples decreased to 70% of their initial height (12 mm (30%) decrease of the initial 40 mm).

After performing the Pfefferkorn test (Figure 2), the pastes were used to print cylindrical specimens with the Lutum® equipment for quality perception at the printing level. Different results were observed for the three pastes used. The initial specimens manufactured with the Gres-130-MP paste presented cracks along the path of extrusion, which led to the addition of water to obtain a workable paste. An

incremental addition of water resulted in the production of a series of specimens with different moisture levels, which demonstrated that a moisture content of 35% is best suited to obtain a printed surface of good quality. The Pfefferkorn tests performed on this mixture resulted in deformations between 5 and 7 mm, i.e. deformations between 12.5% and 17.5%.

3. The calibration between digital and printed models related to dimensions and form

Due to specific physical properties of ceramic materials, such as the fluidity/viscosity of ceramic pastes and the material shrinkage after the firing process, several tests have been conducted in order to infer obtain the optimal printing settings to achieve surfaces of good quality and to identify both geometric and dimensional discrepancies between the digital and the printed models.

This part focused on two sorts of analyses. The first one regards the quality of the extruded surface, considering that a good quality of the printed model consists in a homogeneous extrusion, without excess or scarcity of material, without breaks or settlements resulting from low or excessive moisture, and without air bubbles due to inadequate material compaction. The second analysis is to derive the ability and constrains of the printed model to replicate the dimensions and shapes of the digital model.

3.1. Dimensional analysis

The methodology followed comprised the analysis of two sets of printed models. The first one consisted of twelve specimens of the three aforementioned stoneware pastes, printed using the same digital model, a cylinder with 20 × 40 mm (h × d). The variations between specimens are achieved by combining the different values assigned to the parameters that controlled the printing process: (a) the velocity (displacement) of the extruder's nozzle (mm/s); (b) the pressure applied on the clay cartridge; (c) the height of each printed layer. The objective was to infer the discrepancies between the digital and printed models regarding the influence of these parameters on the height, width and wall thickness.

Other parameters that can eventually be considered in future experiments are the variation of the nozzle diameter, the geometry of the auger inside the extruder and the flow.

Detailed observation of a wide range of printed surfaces makes it is possible to develop knowledge and inspection criteria on imperfections and defects, their causes and recommendations to avoid them. In order to evaluate the dimensional discrepancies between printed and digital models and to correlate them with the parameters, measurements regarding the height, the width and the wall thickness are associated with the values assigned for the printing velocity, the pressure and the layer height.

Figure 4: Set of twelve cylinder specimens (20 × 40 mm), printed with paste Gres-130-MP

Table 1 illustrates the measurements taken of the specimens that were printed with the paste Gres-130-MP, with a moisture content of 34,1wt%. Velocities of 20, 40 and 80 mm/s were tested. The reduction in height is not a failure during the printing process but the typical shrinkage that takes place during the evaporation of moisture out of the ceramics. During the tests an increase in speed resulted in a decrease of height of the specimens. As can be seen in the Table 1, after firing the same decrease in height at

higher extrusion speeds can be observed as before firing. Except that some samples had a higher percentage of shrinkage than others in one direction. In all tests performed, the increase of velocity also corresponded to the decrease of the width of the specimen and the thickness of the walls.

In the tests performed with paste Gres-130-MP the pressure varied between 3.5 and 4.0 Bar. The increment of pressure shows a tendency to augment the height of the printed models. Extrusions performed with higher pressure also result in specimens with larger overall width and thicker walls. This indicates that the auger has not enough internal resistance.

Table 1: Measurements of the printed models with paste Gres-130-MP, after the drying and firing process

Model ref.	Vel. (mm/s)	Press. (bar)	Layer (mm)	Height dried (mm)	Width dried (mm)	Thickness dried (mm)	Height fired (mm)	Width fired (mm)	Thickness fired (mm)
m1	20	3.5	1	18.76	38.57	4.68	16.47	36.04	4.13
m2	40	3.5	1	18.63	37.58	3.86	16.38	35.21	3.53
m3	80	3.5	1	18.44	36.94	3.72	16.35	34.80	3.30
m7	20	4.0	1	18.67	39.33	4.93	16.52	36.78	4.51
m8	40	4.0	1	18.54	39.29	4.86	16.45	36.72	4.47
m9	80	4.0	1	18.62	39.46	5.23	16.42	36.62	4.63
m4	20	3.5	2	18.71	36.61	3.59	16.52	34.18	3.12
m5	40	3.5	2	18.63	36.47	3.50	16.55	34.13	3.08
m6	80	3.5	2	18.62	36.31	3.47	16.52	33.92	3.31
m10	20	4.0	2	18.77	39.33	4.96	16.68	36.37	4.35
m11	40	4.0	2	18.80	38.87	4.81	16.77	36.08	4.32
m12	80	4.0	2	18.78	38.72	4.72	16.70	35.82	4.06

After testing printing processes with layers of 1 and 2 mm height, it was observed that specimens consisting of more layers (higher print resolution in Z direction) resulted in slightly lower objects. Therefore, specimens printed with fewer layers (lower print resolution of 2mm thickness in Z direction), have shrunk less, being closer to the height of the digital model.

The tests that were carried out suggest that for specimens composed with higher layers, the width and wall thickness decrease in dimension, despite being larger than the digital model.

To understand how the samples shrink during firing a volumetric measurement would be more accurate. Also the height is directly influenced by the amount of material extruded and the volume of the test sample. The material must have been flowing through the auger when the pressure is increased, making it hard to draw conclusions on the influence of speed alone.

3.2. Formal analysis

The second set of specimens were made with the objective of inferring the ability and constraints of the printed model and of how to accurately replicate the dimensions and shapes of the digital model. Here for, three series of printed samples were printed, directly corresponding to the next variations in the geometry: straight, semi-curved and curved profiles. In each of the series seven models were realised whose profile inclination varies between angles of 20º and 55º. The specimens were printed with the paste 130-MP mixture with a moisture content of 35wt%, a velocity of 20 mm/s and with a layer height of 1mm (Figure 5).

Invariably, the height of the specimens is smaller than their digital model (Towner [14]). This effect does not occur due to the printing process, since the material is extruded exactly at the desired height as defined in the digital model, but due to the material shrinkage during drying. Nevertheless, the difference is accentuated in models with wider profiles, where there are larger printed areas/surfaces without vertical continuity and consequently with less supporting mass. The material settlement also caused deformations in the bottom and top layers; an effect that was increased in wider profiles. In the first

layers, the weight of the upper layers provoked the settlement of the bottom part, resulting in a more convex profile than defined in the digital model. For the specimens defined by straight profiles and mixed straight and curved profiles, this effect starts to be perceptible at openings with an angle of 40º and is well noticeable at an angle of 45º.

Figure 5: Three series of specimens produced to infer formal discrepancies between digital and printed model

Table 2: Measurements of the printed models with paste 130-MP after firing process

Angle	Arched section		Semi curve section		Straight section	
	Height (mm)	Width (mm)	Height (mm)	Width (mm)	Height (mm)	Width (mm)
20.0º	47.60	42.00	46.23	41.18	44.69	58.81
30.0º	47.77	45.60	46.92	47.93	39.92	71.64
40.0º	47.74	45.77	46.71	55.46	37.78	81.54
45.0º	47.47	48.61	46.02	58.72	33.61	85.46
50.0º	47.75	49.98	47.27	64.76	33.68	90.72
52.5º	47.59	51.62	47.40	67.39	32.15	93.16
55.0º	47.44	52.75	46.78	69.32	31.59	95.56

In the specimens defined by straight profiles, convex deformations are also noticeable in the upper layers. In wider profiles, this effect also results in a form that can be best described as a sinusoidal curve. Such deformation is clearly perceptible in the specimens with 52.5º and 55.0º (upper left image of Figure 6).

3.3 Deformation mechanism

As mentioned before multiple parameters play a role and not all of them were controlled during the tests carried out. The mechanism causing the deformation cannot be directly related to shrinkage caused by the evaporation of moisture if the parameter regarding the material displacement is unknown. The material displacement can influence the behaviour of the fresh extruded clay significantly. The force applied on the layers underneath is an influencing factor, for example, but also the dead load of the material itself. Nevertheless, the research on the deformation is very informative and indicates how to continue.

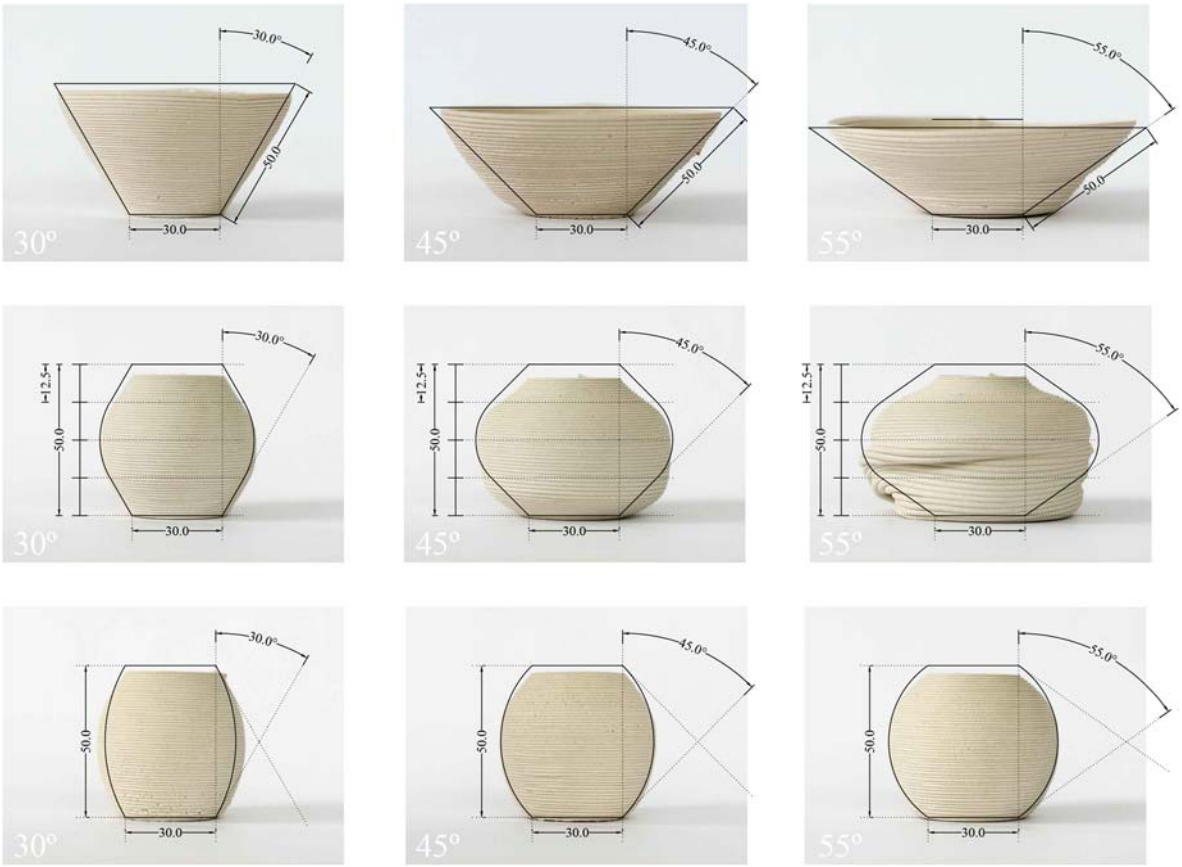

Figure 6: Overlay of the digital model profile over the printed model

4. Digital models and AM of ceramic elements

As showed by authors Kolarevic [15], Oxman and Oxman [16], after the first thoughts and explorations on the role of digital tools in architecture during the last two decades, there is a significant evolution and number of researches on computation and digital fabrication tools in architecture. This evolution has been affecting the formal language of designs, their performative behaviour but also the materialisation of building components. Different terms have been used to describe the integration of computational models in architecture, which are linked to specific functionalities of these models. If the term "algorithmic design" refers to a broad notion on the use of mathematical methods, "generative design" and "parametric design" adds the notion of the possibility of computation to generate new design solutions, or a family of design solutions, by combining different parametric relations between design elements (Klinger and Kolarevic [17]).

4.1. Design customisation through computation

The implementation of computational models in the architectural design process made the customisation of design solutions composed of non-standard elements possible. For the materialisation of these solutions, in contrast to standard building systems, digital fabrication techniques allow and embrace the production of non-standard objects and components (structural, facade, etc.) – process known as mass customisation –, resulting in the possibilities of optimising variance in relation to pre-defined designed criteria (Kolarevic *et al.* [18]). More recently, the term form-finding is being applied to design processes that implement computational models to simulate and generate optimised design solutions regarding single or multi criteria goals. If in the past, design methods were supported by trial and error approaches,

deductive reasoning and accumulated knowledge, form-finding processes are being used to improve the performance of buildings and their components (Oxman and Oxman [16], Kolarevic *et al.* [18]). In recent years, numerous developments in building materials properties are influencing the way architects, engineers and construction professionals foresee improvements in buildings performance (Aksamija [19]).

4.2. Free-form stoneware bricks

What differentiates the most digital controlled AM from mass production systems is the high level of customisation and formal freedom. If we imagine the process of designing and manufacturing a brick, AM is able of breaking with the assumption that the external shape of the brick mainly answers to geometrical requirements, while the inner structure assures the desired performance.

The research presented in this paper proposes an alternative methodology for the conception of this ceramic component. The experiments started with explorations that used a brick with standard dimensions as a reference in which an irregular free-form shape was defined. A set of computational models were defined in Grasshopper®, an API from Rhinoceros 3D®, in order to generate customised inner brick structures. Several geometrical patterns were considered with the aim of establishing comparative performance analysis between them in the next phase of this research. Controllable parameters were defined for all of the patterns, such as the number of cells, in U and V direction, the thickness of the cells walls (relating to the printer's nozzle diameter) and the ability of the patterns to either adapt or not to the defined external shape of the brick.

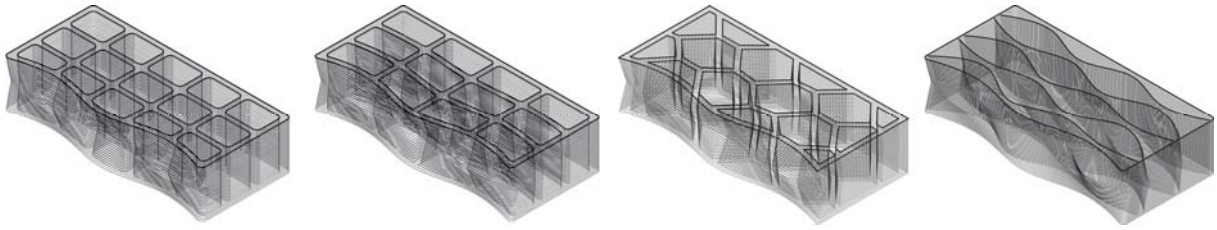

Figure 7: Four design solutions for inner brick structure (quadrangular, hexagonal and curved patterns)

One of the main innovations of this design process is the fact that the computational models and the formal principles of these models take the ceramic fabrication process with thicker extrusion paths into account. In this parametric model that generates the G-code the printer characteristics of the printer used were considered; among them, the material extrusion thickness and path sequence, but also the implementation of constraints regarding the angle of the printed surface. The control and controllability of these settings in the fabrication process is only possible if there is an efficient interface to communicate them to the 3D printer.

4.3. AM G-Code customisation

Due to the non-existence of specific software for the Lutum® 3D clay printer, and the limited control that users have with current 3D printing software, the solution is to interpret the G-Code read by the machine and use it as a starting point. Since most of the information needed to print is embedded in the digital model, it was decided to develop a computational model in Grasshopper® to translate the drawn geometry into G-Code language automatically. The computational model reads the printing paths, orders and decomposes them into X, Y and Z coordinates, and then translates them into the scripting language.

By following the same procedure, data such as the velocity along the extrusion path, speed of additional traveling paths (non-extruding movements) and the extrusion flow is added to the initial G-Code script. The visual control of these data strings allows to assign different printing speeds and flows to different parts of the geometry efficiently, i.e. to assign variations on the finishes and to control the material placement in the overhangs.

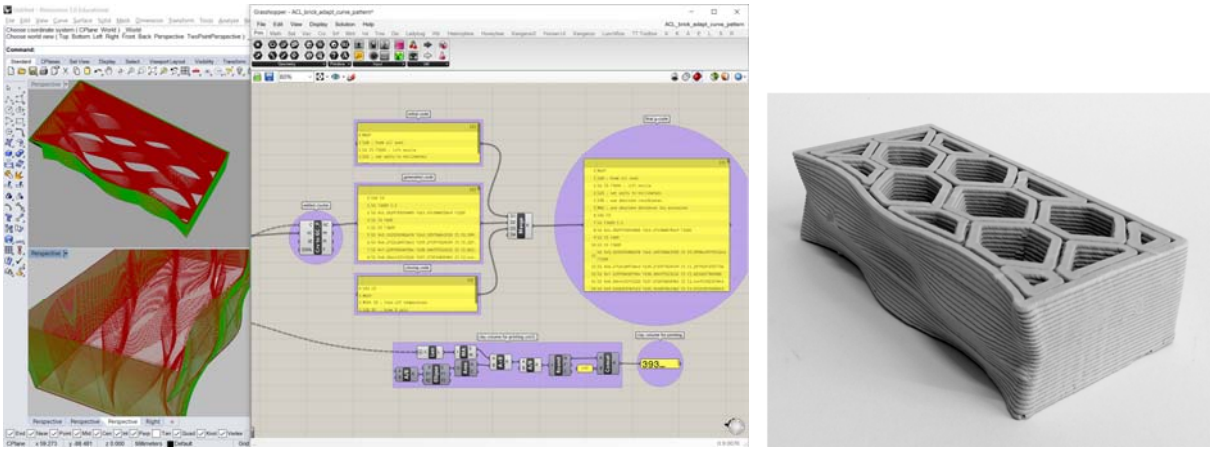

Figure 8: Rhinoceros 3D® model and Grasshopper® API model showing a customised design brick and the generation of the G-Code script for AM. Printed free-form stoneware brick with hexagonal inner structure

5. Conclusions

As referred to, the aim of this paper is to present the main contributions of the ongoing research on the integration of AM in the design and production of free-form stoneware bricks for the built environment.

The Pfefferkorn test showed to be an adequate process for the systematisation of the knowledge of ceramic material properties concerning the inference of the proper plasticity for optimal results in AM processes, for the Lutum® 3D clay printer used at both institutes. Tests with three different ceramic materials were presented. Printing tests with the Gres-130-MP ceramic paste suggested that a moisture content of approximately 35wt% ─ representing a deformation between 12,5% and 17,5% in the Pfefferkorn test ─ is appropriate for reaching an homogenous and smooth printed surface with the hardware used.

By printing a series of specimens from the same cylindrical digital model and by varying the parameters that control the 3D printer within these series, it was possible to clarify the settings of these parameters that result in more significant deviations between the digital and printed models. In summary, it has been suggested that: an increase in extrusion velocity decreases the height, width and wall thickness of the models; in contrast, increase in pressure results in higher, wider and thicker specimens; the height, width and wall thickness of specimens printed with less (but thicker) layers are more similar to the digital model, moreover the finishing surface being less smooth than specimens printed at a higher resolution in Z direction which results in thinner layers.

A series of specimens was produced with the aim of inferring geometrical constrains and formal deviations of the printed models. As synthesis, the results suggested that geometries with constant curvatures are more accurate and profiles with more than 40º of inclination result in major deformations of the shape.

Although influences of differentiating pressure and print speed were noticeable, material displacement needs to be controlled and measured in the next experiments, to obtain accurate information on the mechanism that causes the shrinkage.

Finally, a computational workflow has been described to control the design and fabrication of customised free-form stoneware bricks in an AM production process. The workflow considered both, the properties of the ceramic materials itself and the material related geometrical and dimensional constraints caused by the printer, with the aim of more accurate printing.

The work presented in this paper exposed that, unlike the industrial mass production process, AM of ceramic elements offers a broad geometrical freedom, which can be explored for further application and to experiment with new brick typologies.

Acknowledgements

This work had the financial support of the Project Lab2PT - Landscapes, Heritage and Territory laboratory - AUR/04509 with the financial support from FCT/MCTES through national funds (PIDDAC) and co-financing from the European Regional Development Fund (FEDER) POCI-01-0145-FEDER-007528, in the aim of the new partnership agreement PT2020 through COMPETE 2020 – Competitiveness and Internationalization Operational Program (POCI).

References

[1] Bechthold, M., Kane, A.O. and King, N., *Ceramic Material Systems*. Basel: Birkhäuser, 2015.

[2] Knaack, U., Witte, D., de, Mohsen, A., Tessman, O. & Bilow, M., *Imagine 10 Rapids 2.0.* Rotterdam: nai010 publishers, 2016.

[3] Knaack, U., Klein, T., Bilow, M., Auer, T., *Principles of Construction*. (2nd and revised ed.), Basel: Bikhäuser GmbH, 2014.

[4] Peters, B., Building Bytes: 3D Printed Bricks, in *Fabricate Conference and Publication*, ETH Zurich, Switzerland, February, 2014; 112-119.

[5] Sabin J.E., Miller M., Cassab N., and Lucia A., PolyBrick: Variegated Additive Ceramic Component Manufacturing , in *ACCM 3D Printing and Additive Manufacturing*, June 2014, 1(2): 78-84. doi:10.1089/3dp.2014.0012, 2015.

[6] Cool brick: http://www.emergingobjects.com/project/cool-brick/, 2015.

[7] 3D printed shelter: http://www.elstudio.nl/?p=1639, 2014.

[8] Printed lightweight and very energy efficient façade: http://www.lab3d.nl/, 2016.

[9] Andrade, F.A., Al-Qureshi, H.A. and Hotza, D., Measuring the plasticity of clays: A review. *Applied Clay Science*, 2011; **51**, 1-7.

[10] Pfefferkorn, K., Ein Beitrag zur Bestimmung der Plastizität in Tonen und Kaolinen. *Sprechsaal*, 1924; **57** (25); 297–299.

[11] Gres-130-MP: http://vicar-sa.es/en/, 2017.

[12] Gres-Art13-AT: http://marphil.com/wp-content/uploads/2017/03/GRES-ART13-AT.pdf, 2017.

[13] Creaton N.º 208: http://www.goerg-schneider.de/en/downloads/item/steinzeuggiessmasse-208-datenblatt.html, 2017.

[14] Towner, G. D. The mechanics of cracking of drying clay. *Journal of Agricultural Engineering Research*, 1987; **36.2**; 115-124.

[15] Kolarevic, B., *Architecture in the Digital Age, Design and Manufacturing*. Taylor. 2005.

[16] Oxman, R. and Oxman, R., Performance/Generation: Form Analysis to Informed Synthesis, in (eds.), New York: Routledge, 2014; 97-102.

[17] Klinger, K. R. and Kolarevic, B., *Manufacturing Material Effects: Rethinking Design and Making in Architecture*. Routledge: New York, Oxon, 2008; 6-24.

[18] Kolarevic, Branko, Malkawi and Ali M. *Performative Architecture, Beyond Instrumentality*. Spon Press: New York, pp.86-95, 2005; 194-213.

[19] Aksamija, A., *Integrating Innovation in Architecture: Design, Methods and Technology for Progressive Practice and Research*. West Sussex: John Wiley & Sons, 2016; p. 20-59.